Comparative study for the nondestructive testing of advanced ceramic materials by infrared thermography and holographic interferometry

S. Sfarra[a], C. Ibarra-Castanedo[b], A. Bendada[b], X. Maldague[b], D. Ambrosini[a] and D. Paoletti[a]

[a]LAS.E.R. Laboratory, Dept. of Mechanical, Management and Energy Engineering (DIMEG), University of L'Aquila, Italy, 67100, {stefano.sfarra, dario.ambrosini, domenica.paoletti}@univaq.it
[b]Computer Vision and Systems Laboratory, Department of Electrical and Computer Engineering, Laval University, Quebec City, Canada, G1V 0A6, {IbarraC, Bendada, MaldagX}@gel.ulaval.ca.

ABSTRACT

Advanced ceramic materials are increasingly employed in varied and new applications where improved electrical, mechanical and/or thermal properties are sought. For instance, in a manner similar to carbon or glass fiber reinforced plastics, ceramic matrix composites (CMCs) are designed to improve the naturally brittle characteristics of monolithic ceramics thanks to the inclusion of fibers. Among the main interests for advanced ceramics are the increase in the operation temperature of components, the elimination of the use of cooling fluids, and weight savings. In this paper, the capabilities of infrared thermography and holographic interferometry are investigated and compared for the nondestructive assessment of advanced ceramic materials using three experimental specimens: (1) a monolithic green ceramic tile with fabricated defects, (2) a CMC specimen (from production reject) with a porous alumina matrix reinforced with glass fibers, and (3) a sandwich structure consisting on a carbon fiber honeycomb core with a ceramic plate bonded in one side.

Keywords: infrared thermography, holographic interferometry, advanced ceramics, ceramic matrix composites, carbon fiber honeycombs.

1. INTRODUCTION

Monolithic ceramics are inorganic materials (silicates, oxides, silicides, nitrides, oxynitrides, hybrids, etc.) fabricated by a high-temperature chemical reaction. The properties of a given ceramic compound can be varied, often substantially, by changing its microstructure via differences in fabrication/processing [1]. Modern ceramic materials offer many attractive physical and mechanical properties, such as wear resistance (for industrial applications that involve sliding, rolling, and fluid or particulate flow), chemical resistance (corrosion), high-temperature stability (thermal shock resistance), and thermal barrier properties (bearings, cutting tools, and heat engine components) [2]. Monolithic ceramics are however prompted to fail once their critical stress level is reached due to their intrinsic brittleness.

Ceramic matrix composites (CMCs) have been developed to overcome the brittle nature of monolithic ceramics by adding fillers, *i.e.* reinforcing fibers, to the ceramic matrix. Embedded fibers reinforce the ceramic by deflecting and bridging fractures. Fillers can also be added to the ceramic matrix to enhance characteristics such as electrical conductivity, thermal conductivity, thermal expansion, hardness, corrosion resistance and light weight [3].

Defects in the ceramic body can be originated during the pressing stage (due to the incorrect use of process parameters or to the improper selection of raw materials) or in service conditions. These defects are generally characterized by the inclusion of heterogeneous materials or agglomerates, which decreases the structural strength jeopardizing the final quality of the produced piece. A *green ceramic* (pressed, but not yet dried and fired) is completely recyclable. Inspection at this stage can be therefore very useful.

In this paper, a green ceramic tile, and two CMC specimens were inspected by infrared thermography and holographic interferometry in order to compare results. A brief discussion of the basic principles of infrared thermography and holographic interferometry are presented first.

Thermosense XXXII, edited by Ralph B. Dinwiddie, Morteza Safai, Proc. of SPIE
Vol. 7661, 76610Q · © 2010 SPIE · CCC code: 0277-786X/10/$18 · doi: 10.1117/12.850742

2. PULSED THERMOGRAPHY

Pulsed thermography is a well-know nondestructive testing and evaluation (NDT&E) technique. The basic principle, experimental configuration and advancements have been regularly published in ThermoSense Conferences among others; see for instance reference [4]. For sake of simplicity, only a brief review of the technique is provided herein. Interested readers should consult to the provided references.

In PT, the specimen surface is stimulated with a heat pulse (from a few milliseconds to several minutes) depending on the characteristics or the piece being inspected. The cooling down process is recorded with an infrared camera in a process that could take from a few seconds to several minutes. The acquired data is the processed to improve defect contrast and signal-to-noise ratio. Several processing techniques exist, from a basic cold image subtraction to more advance techniques such as principle components or higher order statistics. The more relevant to the present study are: **differential absolute contrast (DAC)** [5], which calculates the thermal contrast of the actual thermal profiles with respect to a reference area that follows the idealized cooling profile dictated by the Fourier's law 1D solution; **pulsed phase thermography (PPT)** [6], which transforms data from the time domain to the frequency domain in order to obtain phase delay images or *phasegrams* that have an improved defect contrast; **principal component thermography (PCT)** [7], which reorders data taking into account the main variances and reorganize it into new components; and **higher order statistics (HOS)** [8, 9], which calculates the higher order centralized moments (skewness, kurtosis, or n^{th} order moment) of the temporal temperature profiles producing single images summarizing all the relevant information of the original sequence.

The next section describes the holographic interferometry technique.

3. HOLOGRAPHIC INTERFEROMETRY

In general, three forms of holographic interferometry are possible: double-exposure, single exposure real time and sandwich holography. Each of these techniques require a specific arrangement of optical components, depending on what is to be tested and how it is to be loaded or stressed in order to locate a flaw or debond [10].

Double-exposure (DE) and real time (RT) techniques are perhaps the most commonly used; each possessing certain advantages over the others in particular test situations [11, 12]. Figure 1 illustrates the DE and RT configurations.

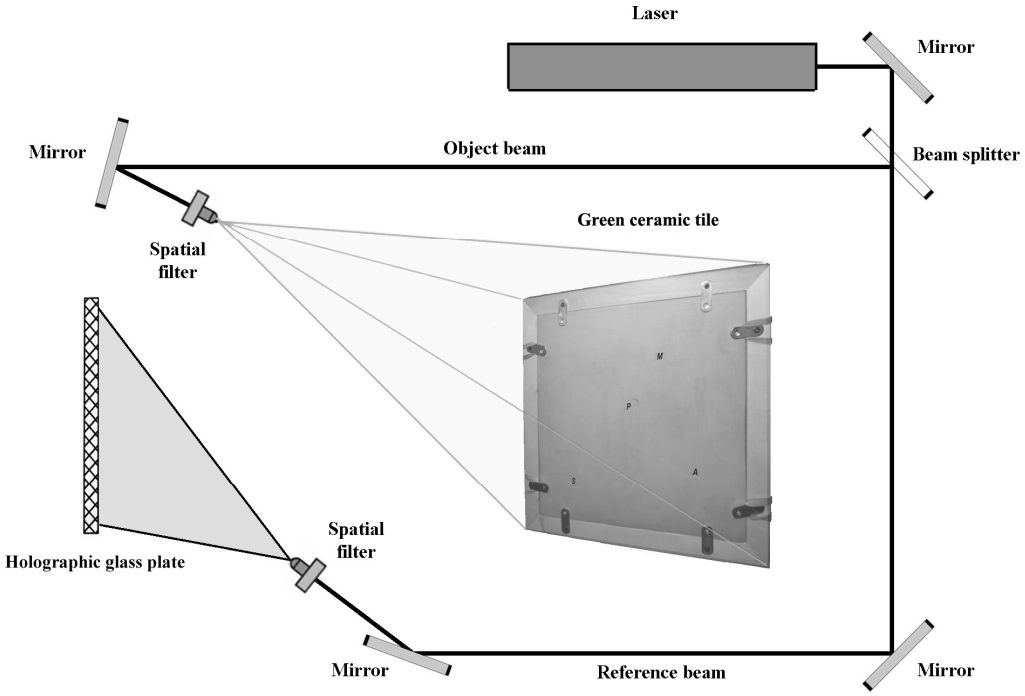

Figure 1. Experimental setup for double exposure (DE) and real time (RT) hologram.

Holographic Interferometry (HI) is a well known tool in NDE [13]. The basic goal of HI is the comparison of an object of interest with itself under different operating conditions. Real Time HI involves the recording of a conventional hologram of the investigated test object, the exact reposition of this hologram in the same position in which it was recorded and the live observation of the formation and evolution of the interference fringes. The main feature of single exposure HI lies in its dynamic nature: the phenomena can be followed in time. The main disadvantages are the reduced fringe contrast (in comparison with double exposure HI) and some practical difficulties, e.g. hologram must be repositioned with a precision in the order of wavelength. In DE two holograms are recorded on the same plate, with each one capturing the object in a different state separated by a fixed time interval (t_i). This technique is less critical than RT HI, because the two interfering waves are always reconstructed in exact register, and the fringes have a good contrast. However, DE is not dynamic and information on intermediate states of the test object is lost.

A detailed study of the fringes allows one to yield information on the behaviour of the object as a whole structure. For a stressed zone of the object without surface geometrical discontinuities, distortions of the fringes indicate abnormal surface deformation and, consequently, the presence of some internal defects. Limits of these techniques include, in general, stringent requirements of mechanical stability for this thus cannot be applied on-line or in an industrial environment.

Holographic Interferometry produces interference between two or more waves, at least one of which is reconstructed by a hologram. The interfering waves may be separated in time. Holographic Interferometry allows measurements, inspection and testing of not only optically flat surfaces but also of any three dimensional surface of arbitrary shape. It also allows interferometric examination of the object in different perspectives. Conventional optical interferometry can be used for optically polished and specularly reflecting surfaces only. If the object is considered to be made up of small mirror elements, then a single holographic interferogram can be equivalent to a large number of observations from a conventional optical interferometry. The holographic interferometry of 3D objects was first introduced by Powell and Stetson [10] almost simultaneously.

The object wavefront can be stored in a hologram and compared with the object after a change that may have taken place. It is this storage or time delay aspect which gives the holographic method a unique advantage over conventional optical interferometry. Horman [14] was the first to suggest the application of a hologram in the test arm of a Mach-Zehnder interferometer. A mechanical or thermal stress must be devised in such a way that the inner defects induce detectable perturbations in the surface deformations. The method and extent of stressing depends on the material property, geometry and dimension of the specimen; and is function of the expected nature of the fault. Finding the best test procedure is partially an empirical process.

4. EXPERIMENTAL RESULTS

4.1 Green ceramic tile

The specimen

A 325x325 mm^2 green ceramic tile (see Figure 2) was produced in the laboratory of a ceramic industry by inserting artificial defects (plastic, aluminum, wood and sponge) during the pressing process, to simulate delaminations or non homogeneities. The specimen contains defects of different sizes (ranging from 20x20 mm^2 to 100x5 mm^2, as depicted in Figure 2), positioned at different depths, z (from 4 to 8 mm).

Infrared thermography results

The ceramic tile was inspected by active thermography using a set of two 250 W lamps (OSRAM SICCATHERM) and a long-wave camera (FLIR S65 HS, 7.5-13 μm, 320x256 pixels). The specimen was heated during 60 s and the surface cooling down was recorded during 180 s, providing 240 thermograms to process.

Results obtained by active thermography are presented in Figure 3. The phasegram shown in Figure 3a corresponds to a frequency of 4.2 mHz and was obtained by processing thermographic data by pulsed phase thermography (PPT). All the fabricated defects (Pe, P, S and A) can be seen in this image, Defect P (plastic) has the greatest contrast, followed by defect Pe (pencil), defect S (sponge) and lastly defect A (aluminum). For the later, the contrast is very weak. These results were to expect given the thermal properties of these materials ($\alpha_P<\alpha_{Pe}<\alpha_S<\alpha_A$). Additionally, a non-fabricated defect, a crack M, was detected as shown in this image.

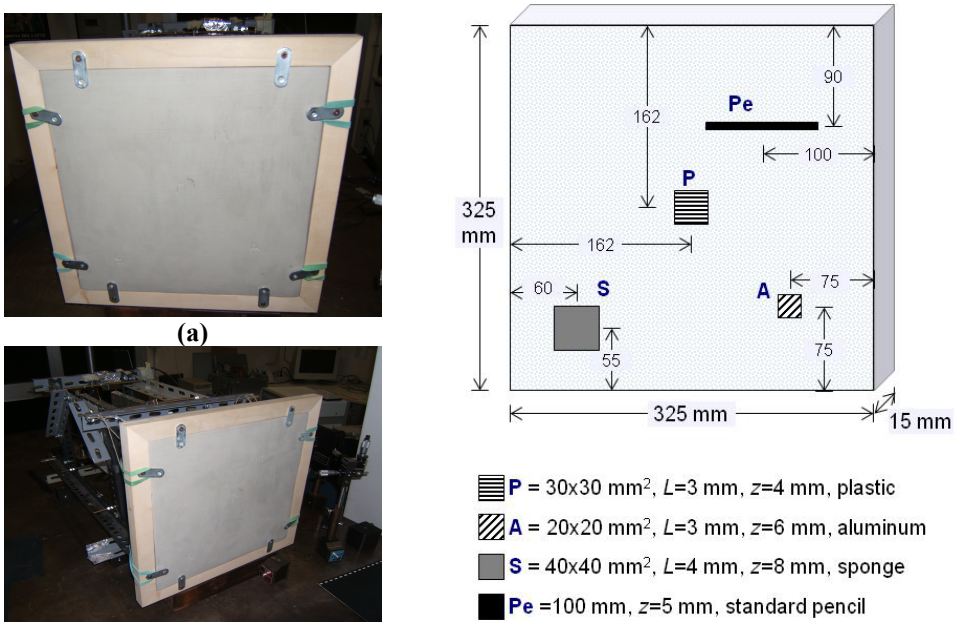

Figure 2. Green ceramic tile (a) front view, (b) side view, and (c) illustration showing the defect size and type and their locations in the ceramic.

Data was also processed using higher order statistical analysis. Figure 3b presents the Kurtosis reconstructed image. This image is interesting and surprising since defects Pe and P are clearly seen as dark areas (as in the PPT phasegram of Figure 3a), while defect S appears as a light spot (contrary to the PPT phasegram of Figure 3a). In addition, defect A and the crack M are practically missing. Statistical analysis could used somehow to discriminate between defect materials. More research is needed at this point though to fully understand these findings.

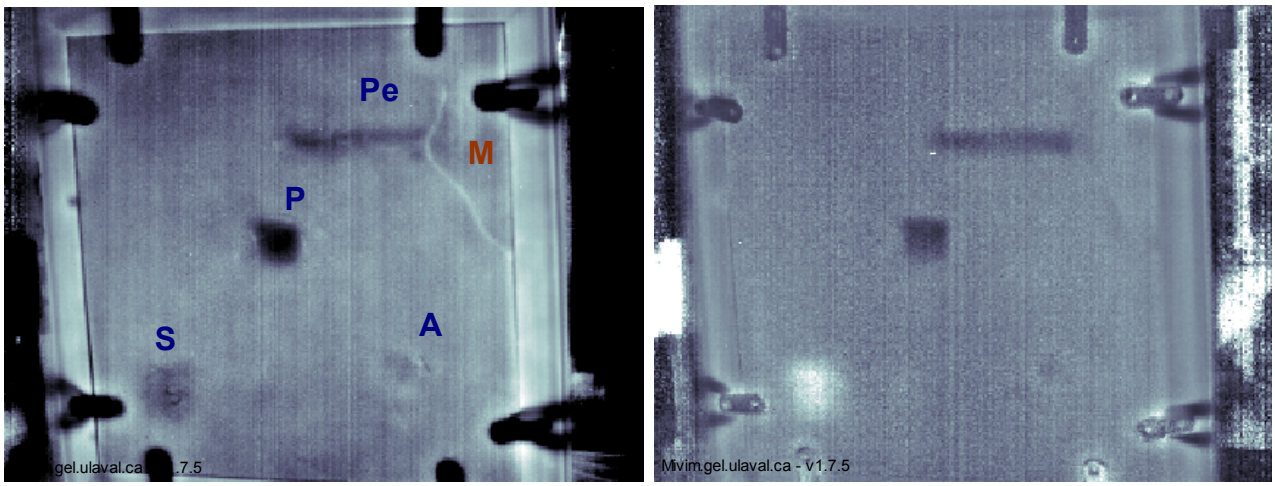

Figure 3. Green ceramic tile PT experimental results: (a) pulsed phase thermography phasegram at f=4.2 mHz showing all defects, and (b) Kurtosis reconstructed image.

Holographic interferometry results

Several interferograms in real time and double-exposure were recorded in order to enhance defect detection and identification; the complexity of the obtained images reveals the influence of many parameters (undesidered movements, spurious fringes due to ambient parameters variations), therefore leaving operator up to select only those which are related to real subsurface flaws, this is a huge task linked to experience and knowledge of the operator.

Figure 4a and Figure 4b show the HI results obtained after stressing the green ceramic tile with a 250 W IR lamp positioned at approximately 50 cm from the inspected surface. Holographic results in Figure 4a have been overlapped to the ceramic material to provide an idea of the actual location of defects Pe, P, S and A in the tile. As can be observed, defect A (aluminum) that simulates a heterogeneous aggregate produces a strong discontinuity, whilst defect S (sponge) produces only a weak discontinuity. Defect P (plastic) can be more clearly seen in the hologram of Figure 4b.

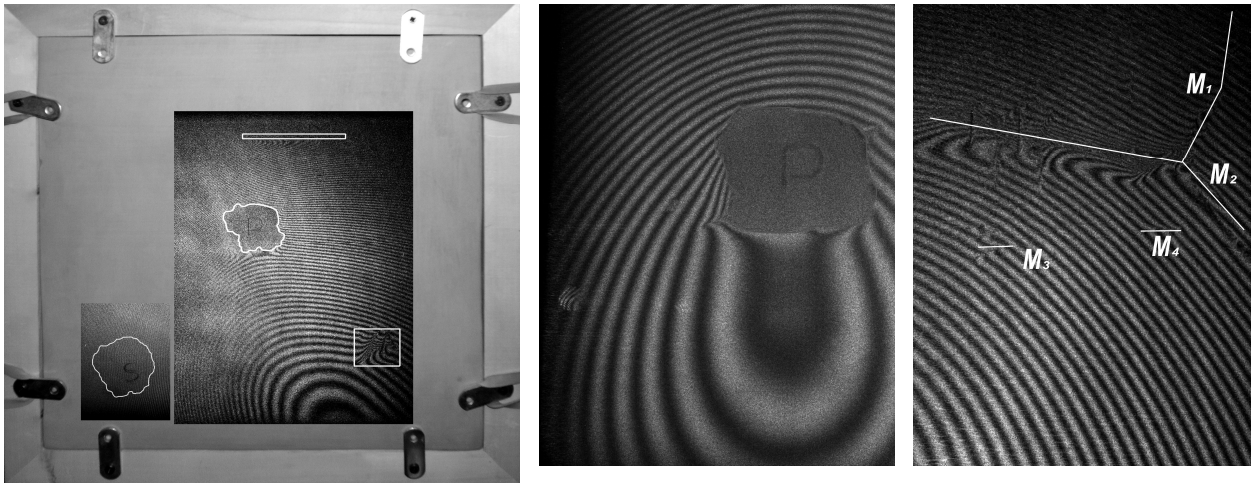

(a) **(b)** **(c)**

Figure 4. Green ceramic tile HI experimental results: (a) double exposure holograms overlaid to a photograph of the ceramic showing defects Pe, P, S and A, (b) double exposure hologram showing defect P, and (c) real time holography showing crack M and "satellites cracks" M_3 and M_4.

The presence of the non-artificially-fabricated crack M, detected by PPT (see Figure 3a), is confirmed as well in Figure 4c. This crack was produced during the fabrication of the tile and confirms the brittleness nature of ceramic materials. Such lack of plastic deformation has inevitably caused an elevated concentration of mechanical stress, provoking some "satellites cracks" (M1, M2, M3, M4) dissipaters of the accumulated energy.

Finally, it is worth noting that although thermography had much difficulties detecting aluminum (given its highly thermal diffusive nature), detection of such material is straightforward by holographic interferometry (as shown in Figure 4a). On the other hand, holographic interferometry is unable to clearly show up the presence of defect S (sponge), which was possible to do by infrared thermography. Furthermore, this kind of defect has a distinctive thermal signature that produced an inverted contrast using higher order statistics (see Figure 3b). These complementarities between both techniques could therefore be conveniently exploited on an integrated approach involving both techniques.

4.2 Porous matrix CMC

The specimen

A second test object coming from production reject is a composite matrix ceramic piece (43x32x12 mm^3) having a porous matrix (see Figure 5a). The porous matrix consists of alumina reinforced with glass fibers. The bonding between a porous matrix and the incorporated fibers typically is weak, thus leading to matrix crack deflection along the fiber-matrix interface. Defects B and D in Figure 5b simulate obstruction of the filter cells, while defect C represents collapsed cells. The filter was inspected exclusively from the top surface (see Figure 5b and Figure 5c).

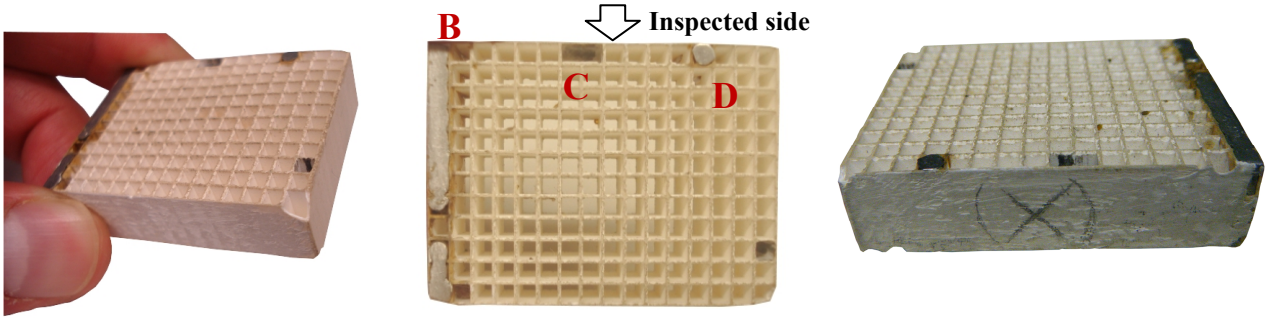

Figure 5. Porous matrix CMC: (a) global view, (b) top view showing defect locations, and (c) view of the inspected side.

Infrared thermography results

The specimen was inspected by pulsed thermography using two photographic flashes (Balcar 6.4 kJ, 5 ms pulses) in reflection mode and a mid-wave infrared camera (Santa Barbara Focalplane, 3-5 µm, 320x256 pixels). Thermographic results are shown on the right column of Figure 6. Figure 6a corresponds to a thermogram obtained by differential absolute contrast (DAC) at t=1.4 s. As can be seen, obstructed cells (defects B and D) appear as dark areas, *i.e.* cold spots, whilst collapsed cells (defect C) appears as a light area, *i.e.* a hot spot. An "(X)" mark, which was written in the surface to indicate the inspected side, is also partially seen in this image. Data was processed by principal components thermography (PCT) as well. Figure 6b and c show the second and third empirical orthogonal functions (EOF), respectively. The former clearly shows the presence of obstructed cells (defect B and D), whilst the later indicates the presence of collapsed cells (defect C). Finally, pulsed phase thermography (PPT) was applied and the phasegram at f=0.7 Hz in Figure 6e was produced.

Holographic interferometry results

Figure 6e shows the holographic results of the CMC specimen. Obstructed cells, defects B and D, appear more evident in this image than the defect C (collapsed cells). In this case, the specimen has been subjected to a thermal stressing induced by a 250 W lamp (OSRAM SICCATHERM) and double exposure HI has been used. The first exposure was made after two minutes cooling, and the second exposure after minute cooling the (P_{laser} = 250 mW, t_{exp} = 2 s + 2 s, t_i = 1 minute).

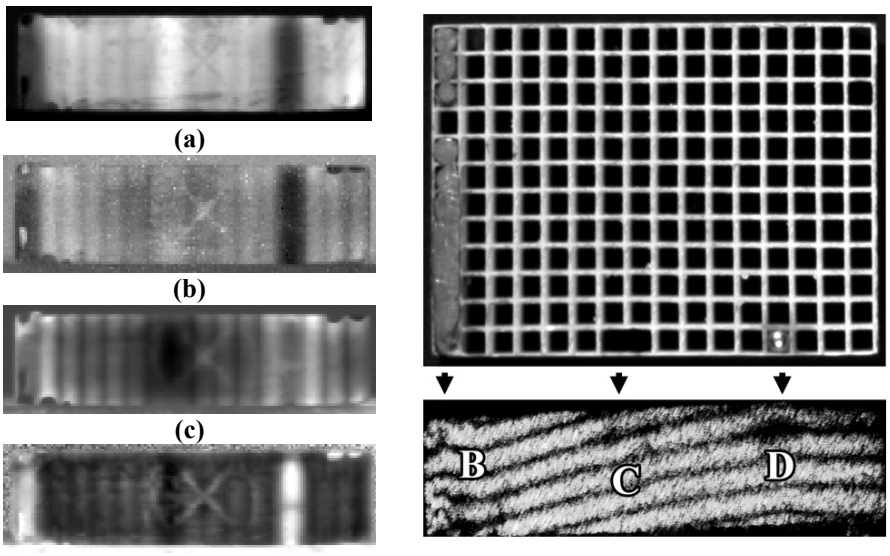

Figure 6. Porous matrix CMC experimental results: (a) DAC thermogram at t=1.4 s, (b) PCT EOF_2, (c) PCT EOF_3, (d) PPT phasegram at f=0.7 Hz, and (e) specimen photo and DE HI result.

4.3 Sandwich CMC/carbon fiber specimen

The specimen

The materials that constitute the specimen (102x102x7 mm^3) were provided by Thales Alenia Space. They consists of a carbon fiber honeycomb core between two CFRP layers (0, 90) skins (thickness = 6 mm), defined as triax HC, bonded in a side by double sided adhesive tape with a ceramic plate in alumina (thickness = 1 mm). See Figure 7a and 7b. The specimen core was pierced from the side 1 (defects A and C as seen in Figure 7b and c) in our laboratories. The fabricated holes have the same diameter (φ=5 mm), and size (L=70 mm), and were pierced to the same depth (z=4 mm deep from the top). Both holes have been filled with two sponges covered by Teflon with the purpose to simulate inclusions. A portion of honeycomb (10x11 mm^2, defect D in Figure 7a) has been removed with the purpose of simulating a loss of material after an impact.

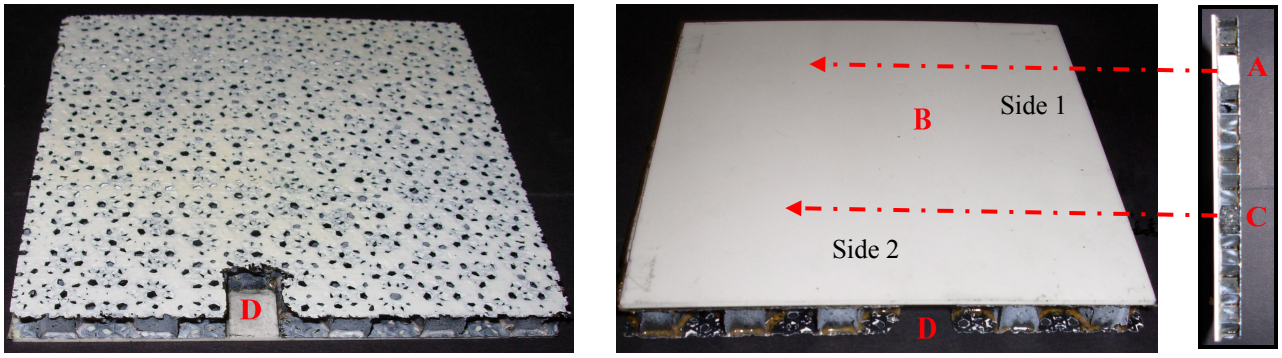

(a) (b) (c)

Figure 7. Sandwich CMC/carbon fiber specimen (a) rear view showing the sandwich structure, (b) top view showing the approximate location of defects A, B, C and D, (c) lateral view showing the cross-section of fabricated defects A and C.

Infrared thermography results

Figure 8 presents some results obtained by infrared thermography. Figure 8a shows a phasegram obtained after processing data from a reflection mode experiment using two photographic flashes. As can be observed, only defect D can be identified. Much more energy would be required in reflection mode in order to be able to detect defects A and C and to improve contrast of defect D. This is mainly due to the thermal properties of the ceramic material that acts as a resistance to the thermal front. In reflection mode, heat propagates from the surface to the defects locations and then it travels back to the specimen surface. The situation would be different in transmission mode. In this case, heat would travel from the rear surface to the front, considerably reducing the energy requirements for defect detection.

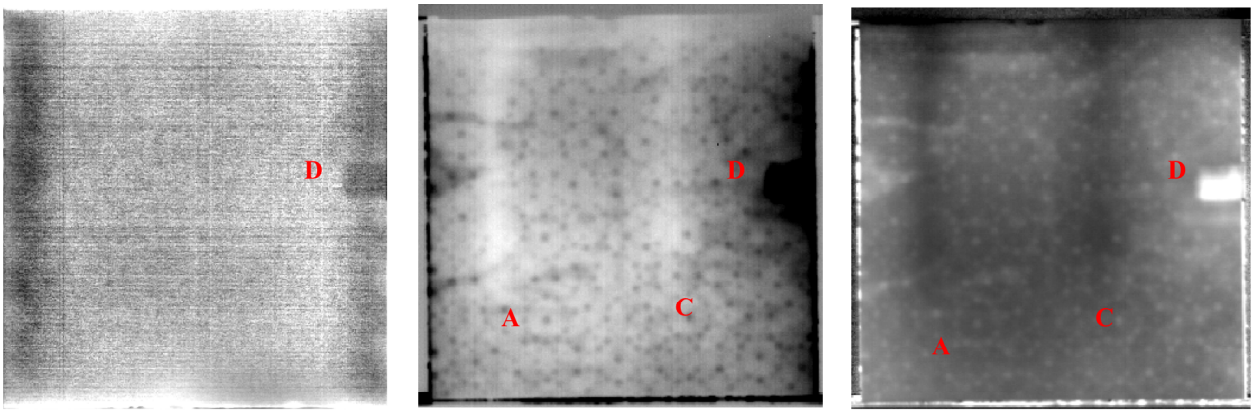

(a) (b) (c)

Figure 8. Sandwich CMC/carbon fiber specimen PT results: (a) PPT phasegram f=0.02 Hz from reflection mode, (b) PCT EOF_3 in transmission mode, and (c) PPT phasegram at f=0.014 Hz in transmission mode.

The specimen was hence inspected in transmission mode. Heating time was 1 minute with two halogen lamps and data was processed by PCT and PPT. The third empirical orthogonal function (EOF_3) obtained by PCT is presented in Figure 8b. In this case, defects A, C and D are detected. The honeycomb structure can also be seen. A PPT result is shown in Figure 8c, in which the same features can be seen.

Holographic interferometry results

A continuous-wave laser (λ = 532 nm) of 250 mW power was employed as the source of coherent light. Holographic interferograms were recorded under thermal loading. In the first analysis with the DE technique, interferograms were recorded after the sample had been heated by a welder (P_{max} = 400 W) positioned in transmission mode near the honeycomb surface. The specimen has been cooled in air between exposures. Figure 9a show the trend of the holographic fringes for the sample cooled in air (t_{exp}=0.9 s, t_i=3 s). As can be seen, the trend of fringe pattern is regular to the left, but to the right there is a bending relatively to the defect C and with greater evidence for the defect D; therefore, the presence of defects is indicated by discontinuities in the fringe system, but the exact outline of the defect cannot be discerned. By varying the cooling period, the surface temperature of the second exposure changes and consequently, the fringe number varies. In particular, a decrease in temperature change causes a reduction in the number of fringes; in fact, by increasing the time interval between the exposures (t_{exp}=0.9 s, t_i=5 s) in order to reach a greater temperature change, the fringe pattern of Figure 9b is obtained. The trend of the fringes is the same, but their marked distortions show more clearly the location and extension of the defect D.

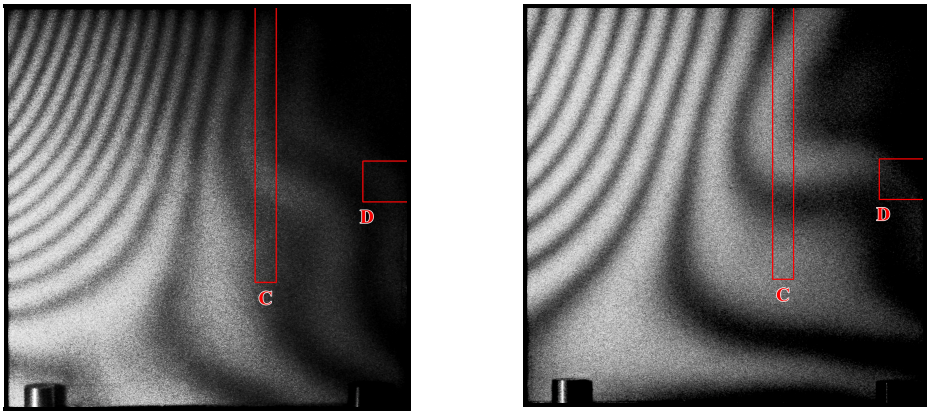

(a) **(b)**

Figure 9. Sandwich CMC/carbon fiber specimen double exposure interferograms showing defects C and D, thermally stressed by a welder and cooled down in air (a) t_i = 3 s, and (b) t_i = 5 s.

Under these conditions, we have not been able to find evidence of defect A, probably due to the different stopper (see Figure 7) inserted in the defect C in comparison to defect A, with different repercussion on the heat transmission and therefore on the detectable perturbations in the surface deformation. Besides, the Teflon layer that covers the inserted sponge in defect A, is slightly thicker than the layer that covers the inserted sponge of defect C. Additionally, a non-fabricated anomaly, defect B was also detected. Real time holographic interferometry was used in this case using heating forced convection (t_{exp}=1 s) as a stress mechanism. Two experimental results recorded at cooling times (Figure 10a and 10b) were obtained (with a longer cooling time, the defect B becomes more evident). From these figures, it can be observed that the fringe patterns kept their uniformity, except where the defect B appears. Presumably, the cycles of heating and cooling used, a precedent weakness point of the material and a low resistance of the material to important thermal shocks, have produced this real defect inherent the ceramic material.

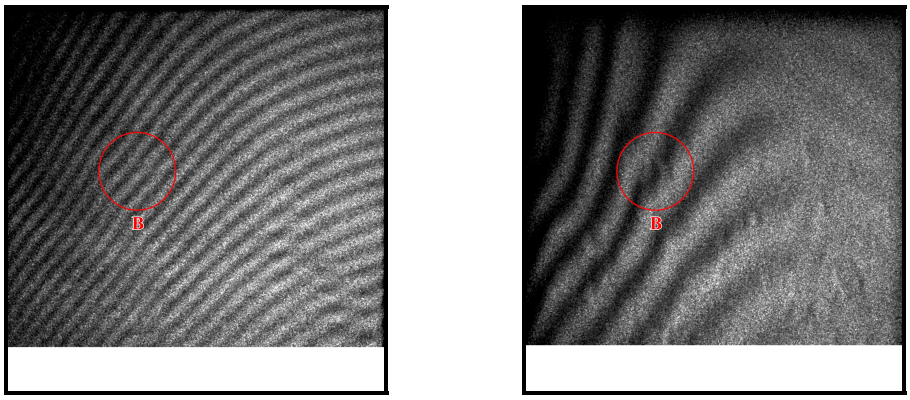

(a) **(b)**

Figure 10 a) and b). Real time holographic interferograms showing non-artificially fabricated defect B after cooling in air.

5. CONCLUSIONS

NDT is an important aspect in the manufacture of CMC structures and Ceramic Materials. Infrared thermographic and holographic interferometry can be considered as attractive tools for the non-destructive evaluation of materials; the choice of the most appropriate technique mainly depends on the particular material and the specific requirements of the quality control process.

The damage mechanisms that occur in material during failure are not yet fully understood, requiring extensive analysis to ensure the manufacturing of intact structures. Furthermore, the high costs of CMC structures and their use in safety relevant applications require the integration of NDT methods, not only to ensure the integrity of the manufactured CMC structures, but also as a useful tool to analyze the manufacturing process for optimization and improvements. Each of the introduced methods has its advantages and disadvantages.

The thermographic technique has shown greater sensibility in detecting the defect S (sponge) in the green ceramic tile, while the holographic technique provided a clearer image of defect A (aluminum) and furnished a more accurate result for the non-fabricated defect M (M_1 and M_2) (crack).

For the porous matrix CMC, the thermographic result for the defect C is more evident than the holographic result, while the defects B and D are confirmed.

Finally, results for the sandwich CMC/carbon fiber specimen provided some interesting results. Defect D (detach region) was the easiest one to detect by both, infrared thermography (in reflection and transmission modes), and double exposure holographic interferometry. Defects A and C, consisting of perforated holes filled with a combination of sponge and Teflon, were detected by infrared thermography in transmission mode. Strangely, only defect C was detected by holographic interferometry, even though both defects were fabricated in a similar manner. This odd result could be explained by the differences in the Teflon layer that covers the inserted sponge in defects A and C and by the insertion of a outer stopper for the defect C. In addition, a non-fabricated anomaly (defect B) could only be detected by HI.

As a final conclusion, the integration between thermographic and holographic techniques can be though as an interesting tool for the NDT inspection of ceramic materials (traditional and advanced) due to the complementarities shown in the present study.

ACKNOWLEDGEMENTS

Authors want to thank the support of the Chaire de recherché du Canada (MIVIM), the Ministère du développement économique, innovation et exportation du Québec, the Ceramiche San Bernardino Laboratory for the preparation of the green ceramic tile, in particular Miss Stella Lucente and P. Montanari, F. Pastorelli and M. Tursini of Thales Alenia Space – L'Aquila – for providing the ceramic plate in alumina and the sandwich structure with the relative technical characteristics.

REFERENCES

1. Rice R.W. *Ceramic Fabrication Technology*, Marcel Dekker, Inc., U.S.A. 2003.
2. Taylor T.A., Bergeron C.G. and Eppler R.A., *Ceramic coatings*. In Metals Handbook, 9th edn, Vol. 5, T.B. Zorc, Metals Park, OH, 1982, pp. 532 – 547.
3. Wessel J. K. *Handbook of Advanced Materials*, James K. Wessel (ed.), John Wiley & Sons, Inc., 2004.
4. Ibarra-Castanedo C., Avdelidis N. P., Grenier M., Maldague X. P. and Bendada A. "Active thermography signal processing techniques for defect detection and characterization on composite materials," *Proc. SPIE - The International Society for Optical Engineering, Thermosense XXXII*, Orlando, FL, April 5-9 2010, Eds. Ralph B. Dinwiddie and Morteza Safai, Paper **7661-24**.
5. Pilla M., Klein M., Maldague X. and Salerno A., "New Absolute Contrast for Pulsed Thermography," *Proc. QIRT 2002*, D. Balageas, G. Busse, G. Carlomagno (eds.), pp. 53-58, 2002.
6. Maldague X. P. and Marinetti S. "Pulse Phase Infrared Thermography," *J. Appl. Phys.*, **79**(5):2694-2698, 1996.
7. Rajic N. "Principal component thermography for flaw contrast enhancement and flaw depth characterization in composite structures," *Compos. Struct.*, **58**:521-528, 2002.
8. Madruga F. J., Ibarra-Castanedo C., Conde O. M, Maldague X. P. and Lopez-Higuera J. M "Enhanced contrast detection of subsurface defects by pulsed infrared thermography based on the fourth order statistic moment, kurtosis," SPIE - The International Society for Optical Engineering, Thermosense XXXI, Orlando, FL, April 13-17 2009, Eds. Douglas D. Burleigh and Ralph B. Dinwiddie, 7299:72990U.
9. Madruga F. J., Ibarra-Castanedo C., Conde O. M, Lopez-Higuera J. M and Maldague X. P. "Automatic data processing based on the skewness statistic parameter for subsurface defect detection by active infrared thermography," *Proc. QIRT 9 – Quantitative Infrared Thermography*, [CD-ROM], Krakow, Poland, July 2-5, 2008.
10. Stetson K.A. and Powell R.L. "Hologram Interferometry," *J. Opt. Soc. A.*, **56**, 1161 – 1163, 1966.
11. Paoletti D., Schirripa Spagnolo G., "Interferometric methods for art work diagnostics", *Progress in Optics*, **35**, 197-255, 1996.
12. Ambrosini D., Paoletti D., "Holographic and speckle methods for the analysis of panel paintings. Developments since the early 1970s", *Review in conservation*, 5, 38-48, 2004.
13. Vest C.M., "Holographic Interferometry", Wiley, New York, 1979.
14. Horman M. H., "An application of Wavefront Reconstruction to Interferometry", *Appl. Opt.***, 4**:333-336, 1965.
15. Di Ilio A., Paoletti A. and Paoletti D., *Holographic tests on ceramic coatings on metal surfaces*, *Short Communication, Composites Science and Technology*, **57**, 365-369, 1997,